Electronic Supplementary Material (ESI) for Soft Matter.
This journal is © The Royal Society of Chemistry 2017

Supplementary Information (ESI) for Soft Matter

Biological Plywood Film Formation from Para-nematic Liquid Crystalline Organization

Oscar F. Aguilar Gutierrez[a] and Alejandro D. Rey[a*]

[a]*Department of Chemical Engineering. McGill University 3610 University St. Montreal, Quebec, H3A 0C5, Canada*
[*]*Corresponding author: alejandro.rey@mcgill.ca*

Appendix A

This appendix presents mathematical details for the derivation of the integrated phase ordering-mass transfer model based on the Landau-de Gennes **Q**-tensor theory and the anisotropic mass diffusion equation in time-dependent geometry. The mathematical description of liquid crystals used in this paper is at the mesoscopic scale and is written in terms of the second moment of an orientation distribution function (ODF) which is the definition of the **Q** tensor as expressed in eqn. (S.1 a-b):

$$\mathbf{Q}=\int\left(\mathbf{uu}-\mathbf{I}/3\right)\rho(\mathbf{u})d^2\mathbf{u};\mathbf{Q}=\mathbf{Q}^T;tr(\mathbf{Q})=0$$
$$\mathbf{Q}=S\left(\mathbf{nn}-\frac{\mathbf{I}}{3}\right)+P\left(\mathbf{mm}-\mathbf{ll}\right) \qquad \text{(S.1 a-b)}$$

This symmetric and traceless tensor can be parameterized in terms of the director triad vectors **n, m, l** and two scalar order parameters (S,P) that result from a linear combination of the eigenvalues **Q**. The unit vector **n** is known as the director or average orientation and S is known as the uniaxial scalar order parameter. From equation (S.1a) we find: $\mathbf{Q}:\mathbf{nn}=2S/3;\mathbf{Q}\cdot\mathbf{n}=2S\mathbf{n}/3$. Specific components of **Q** such as Q_{xx} are found from: $Q_{xx}=\mathbf{Q}:\boldsymbol{\delta}_x\boldsymbol{\delta}_x;\boldsymbol{\delta}_x\cdot\boldsymbol{\delta}_x=1$. Likewise n_x is found from

$\mathrm{n_x} = 3\mathbf{Q}:\mathbf{n}\boldsymbol{\delta}_x / 2S$.

The total free energy density f can be expressed as the sum of the homogeneous contribution which is a Landau expansion in terms of appropriate invariants of **Q** and proportional to the so-called nematic potential U. This nematic potential U is a dimensionless concentration with respect to the critical phase transition volume fraction. The second contribution to the free energy is known as the elastic free energy from modes of deformation, each associated to an elastic constant L_i. For chiral mesogens we consider two terms, one related to the twist deformation and intrinsic chirality associated to L_1 and the second encompassing other common modes of deformation and are associated to L_2. The total free energy F is given in eqn. (S.2 b):

$$F = \int_V f dV; \frac{f}{ck_BT} = \frac{1}{2}\left(1-\frac{U}{3}\right)\mathbf{Q}:\mathbf{Q} - \frac{U}{3}(\mathbf{Q}\cdot\mathbf{Q}):\mathbf{Q} + \frac{U}{4}(\mathbf{Q}:\mathbf{Q})^2 + \frac{L_1}{2ck_BT}\left[\nabla\times\mathbf{Q} + \frac{4\pi}{p_o}\mathbf{Q}\right]^2 + \frac{L_2}{2ck_BT}\left[\nabla\cdot\mathbf{Q}\right]^2 \quad \text{(S.2 a-b)}$$

where F is the total free energy and f the free energy density. The evolution drives the system to the minimum energy given the initial configuration and a given set of boundary constraints. Even when the evolution of liquid crystalline materials can be given in terms of **n**, **m**, **l**, S and P, it is more convenient to derive the model using directly the components of **Q** and later extract such information from their definitions, which is the approach adopted here. Given the fact the **Q** tensor is not a conservative field, it follows the Langevin-type dynamics where the time derivative of **Q** is proportional to the so-called molecular field, which is the functional derivative of the total free energy with respect to variations in **Q**: $\left[\delta F / \delta \mathbf{Q}\right]^{s]}$, where [s] denotes symmetric and traceless. The pre-factor corresponds to the mobility as expressed in eqn. (S.3 a):

$$\frac{\partial \mathbf{Q}}{\partial t} = -\frac{6\overline{D_r}}{ck_BT}\left[\frac{\delta F}{\delta \mathbf{Q}}\right]^{[s]}; \left[\mathbf{M}\right]^{[s]} = \frac{1}{2}\left(\mathbf{M} + \mathbf{M}^T - \frac{2}{3}tr(\mathbf{M})\right)$$
$$\overline{D_r} = \frac{D_r}{\left(1 - \frac{3}{2}\mathbf{Q}:\mathbf{Q}\right)^2} \qquad \text{(S.3 a-b)}$$

Where $\overline{D_r}$ is the variable rotational diffusivity and D_r is the bare, single-rod, rotational diffusivity (with reciprocal time dimension i.e. [=] 1/time), c the number of molecules per unit volume, k_B the Boltzmann constant, T the absolute temperature. The distinguishing feature of the model derived for this paper is the variable nematic potential $U(\mathbf{x},t)$ which is a function of the solvent volume fraction $\varphi_w(\mathbf{x},t)$. Therefore the information resulting from changes in the mass transfer equation for the solvent φ_w are introduced to the $\mathbf{Q}(\mathbf{x},t)$ tensor dynamics through the nematic potential . On the other hand, the mass transfer equation for the solvent is written in terms of the divergence of the mass flux. We consider here an anisotropic constitutive equation with an isotropic D_{iso} and anisotropic D_{ani} diffusivity constants. This anisotropic relationship include gradients in the solvent concentration and a bilinear function of $\mathbf{Q}$ and ∇c_w as expressed in eqn. (S.4 a-b):

$$\frac{\partial c_w}{\partial t} = -\nabla \cdot \mathbf{j}_w; \mathbf{j}_w = -\left(D_{iso}\nabla c_w + D_{ani}\mathbf{Q}\cdot\nabla c_w\right);$$
$$D_{iso} = \frac{D_{\parallel} + 2D_{\perp}}{3}; D_{ani} = D_{\parallel} - D_{\perp} \qquad \text{(S.4 a-d)}$$

To derive the equation that takes into account the overall total volume reduction due to water loss from the system, we use the mesogen mass conservation within the film.

$$\frac{d}{dt}\int_{V(t)} c_c dV = 0; \rho_c \frac{d}{dt}\int_{V(t)} \varphi_c dV = 0$$
$$\int_{V(t)} \frac{\partial \varphi_c}{\partial t} dV + \int_{S(t)} \varphi_c \mathbf{v}\cdot\mathbf{k} dS = 0 \qquad \text{(S.5 a-c)}$$

where c_c is the mesogen mass concentration, **v** the velocity of the control volume and **k** the unit normal to the corresponding surface. The first term on eqn. (S.5 c) can be expressed in terms of the divergence of the flux of the solvent, which then can be transformed to an integral form by using Gauss' integral transformation. Such integral is then evaluated at the relevant surfaces and by making use of the cross-section average definition $\langle A \rangle(t) = \frac{\int_S A(\mathbf{x},t)dS}{\int_S dS}$ furnishes the equation for the film thickness h(t) (in the vertical direction):

$$\frac{dh}{dt} = \frac{2h(t)}{\rho_w L}\left\langle j_z^{\,wall} \right\rangle(t) \tag{S.6}$$

The physical interpretation of eqn. (S.6) is given as follows: the rate of change of the film thickness is proportional to the flow of water leaving the film through the side boundaries of the geometry, however this flow depends on the order of magnitude of the average surface flux multiplied by its respective cross section which is being modified (it decreases) as the film shrinks vertically. The integrated phase ordering/mass transfer model in an evolving geometry is given by equations S.3-S.6 and is solved numerically using finite element methods as discussed in the paper. The number of differential equations are five partial differential equations for the **Q**-tensor, one partial differential equation for c_w, and one ordinary differential equation for h, for a total of seven differential equations.

Appendix B.

This appendix provides details regarding the particular values of the nematic potential *U* and its impact on the homogeneous free energy. When the homogeneous free energy is expressed in terms of the scalar order parameter *S*, the particular value of *U* provides with the shape to the function

and hence indicate the stable thermodynamic state in terms of S. For collagen solution p_o has a small effect on stability thresholds and is not discussed here; see [7]. The isotropic state is stable when U is low and the free energy has only one minimum. Increases in U change the shape of the free energy and a second minimum is obtained yet of higher energy than the isotropic state. The particular value where the second minimum appears is $U^{**} = 8/3$. Further increases in U lead to a stable ordered state when the second minimum is a lower energy state and the range between 8/3 and 2.7 corresponds to local metastable state and the upper bound is denoted as U_{IC} and indicates both minima have the same energy, thus both states: the disordered and ordered are stable. Higher values indicate the ordered state is the stable state and the concentration denominated as U* is the metastable limit. These values are depicted in figure S1.

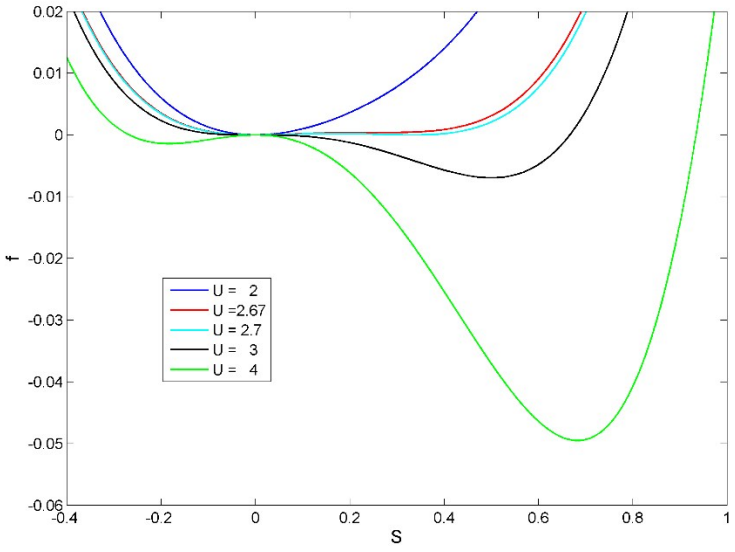

Figure S1. Homogeneous free energy as a function of the scalar order parameter for varying nematic potential U.

Appendix C.

This appendix presents additional plots and surface plots to support the discussion in section 4. We first present a detailed figure where the height of the film is plotted as a function of time in figure S2 for varying Π as indicated in the legend.

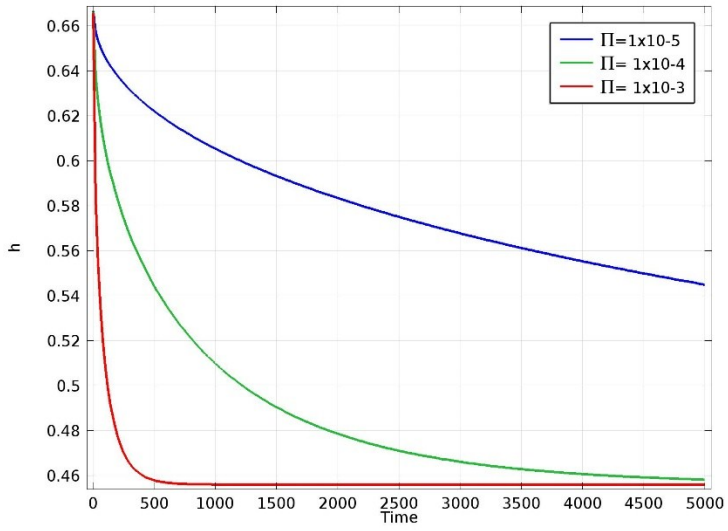

Figure S2. Film height as a function of time as the film dries.

The figure shows that the exponential decay of h(t) increases its rate as the time scale ratio Π increases. The intermediate green curve corresponds to the synchronized phase ordering-water removal mode that yield a defect-free film. The lower (blue curve) and faster (red curve) decays lead to cellular patterns and polydomain patterns, respectively.

Next we discuss the film patterns in the three regimes: monodomain, monodomain-cellular, and polydomain modes. To elucidate the underlying mechanisms it is best to use different quantities related to the **Q**-tensor (phase ordering) and choose the scalar order parameter S(y,z,t), and $Q_{xx}(y,z,t)$, $=\mathbf{Q}:\boldsymbol{\delta}_x\boldsymbol{\delta}_x$. For the water removal rate and thermodynamic transitions we use the mesogen dimensionless concentration U(y,z,t) and the two non-zero components of the mass flux vector

J(y,z,t). We wish to show evidence that when the time scale ratio is lower $\Pi < \Pi^*$ or higher $\Pi > \Pi^*$ than the critical value $\Pi^* \sim O(10^{-4})$, a perfectly aligned helix does not emerge, simply because the water withdrawal rate is either too slow (monodomain-cellular mode) or too fast (polydomain mode), in qualitative agreement with experiments.

(i) Monodomain Transition Mode ($\Pi^*=10^{-4}$)

Figure S3 shows the surface plots of S and $|n_x|$ for increasing times as indicated in figure 4 and the curves shown in figure 5 are extracted from the presented surfaces at the halved height of the computational domain. The upper figures S.3 show a planar stable phase ordering front and a decrease in h. The bottom figures S.3 show that the director remains aligned in the interior and that it is compatible with the helical front moving from the edges towards the interior.

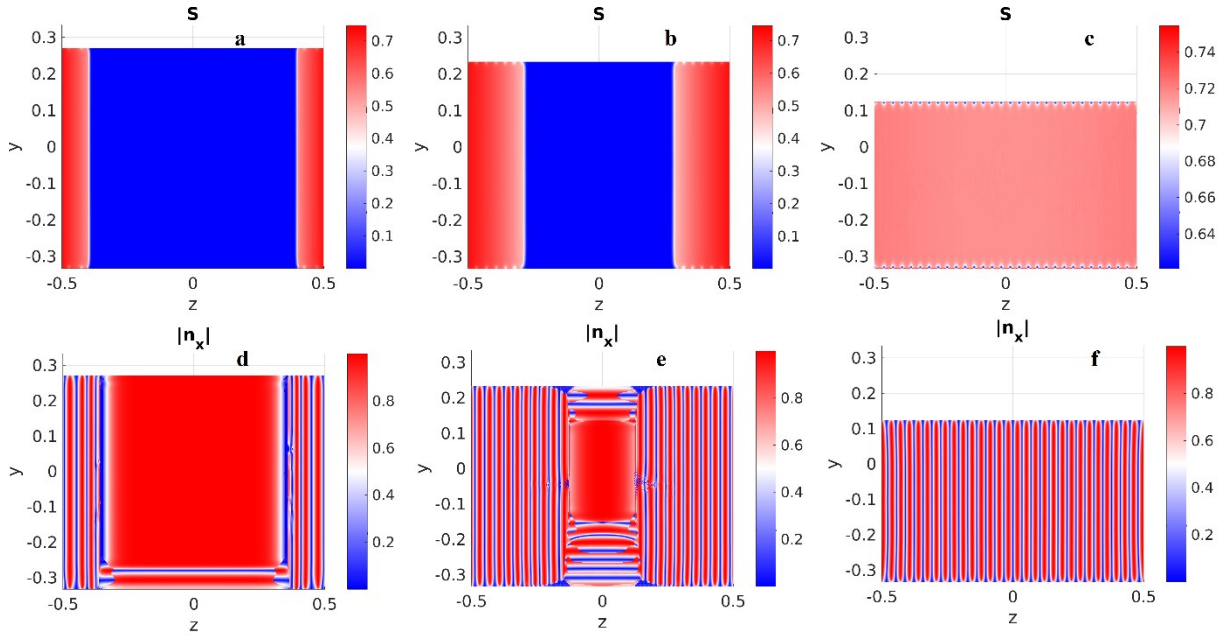

Figure S3. Scalar order parameter S (a-c) and out of plane component of the director n_x (d-f) for increasing times as indicated in figure 5, showing a relaxation of S in regions where the stability threshold (U=3) has not been reached but the para-nematic director persists leading to a homogeneous helical axis. Monodomain mode for $\Pi = \Pi^*=10^{-4}$.

(ii) Monodomain-Cellular Mode ($\Pi<\Pi^*=10^{-4}$)

Figure S4 shows the surface plots of the microstructure in terms of Q_{xx} and the change in the mesogen concentration U for increasing times as indicated in figure 6. These surface plots show the appearance of the cellular zone due to the presence of a presence of a pre-cholesteric state close to the central region as observed in figure 6.

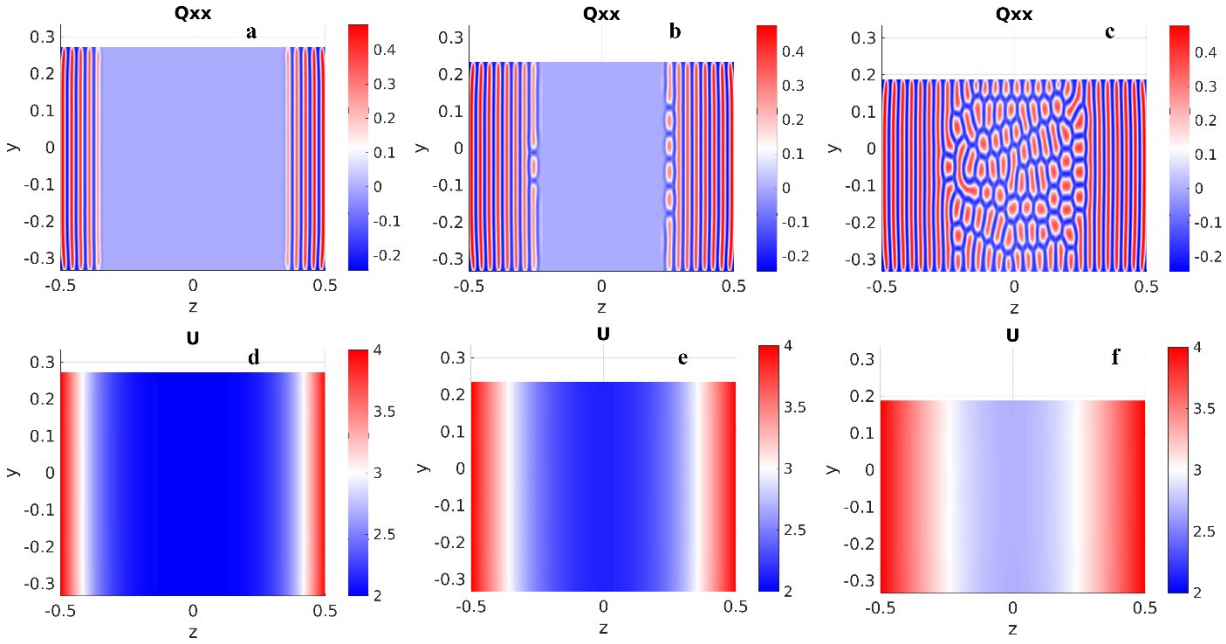

Figure S4. Q_{xx} surface plot in terms of the spatial coordinates *y*-*z* (a-c) for increasing times (t^* = 1000, 3000, 8000) in the simulations and the nematic potential *U* (d-e) for the same times for $\Pi = 1\text{x}10^{-5}$ showing a homogeneous helical axis forming from the edge toward the central region of the cross section.

(iii) Polydomain Mode ($\Pi>\Pi^*=10^{-4}$)

Figure S5 are analogue surface plots to figure S4 for $\Pi = 10^{-3}$ and shows the inhomogeneity in the helix formation due to fast diffusion. The curves associated to the presented microstructure and mesogen concentration surfaces are presented in figure 7.

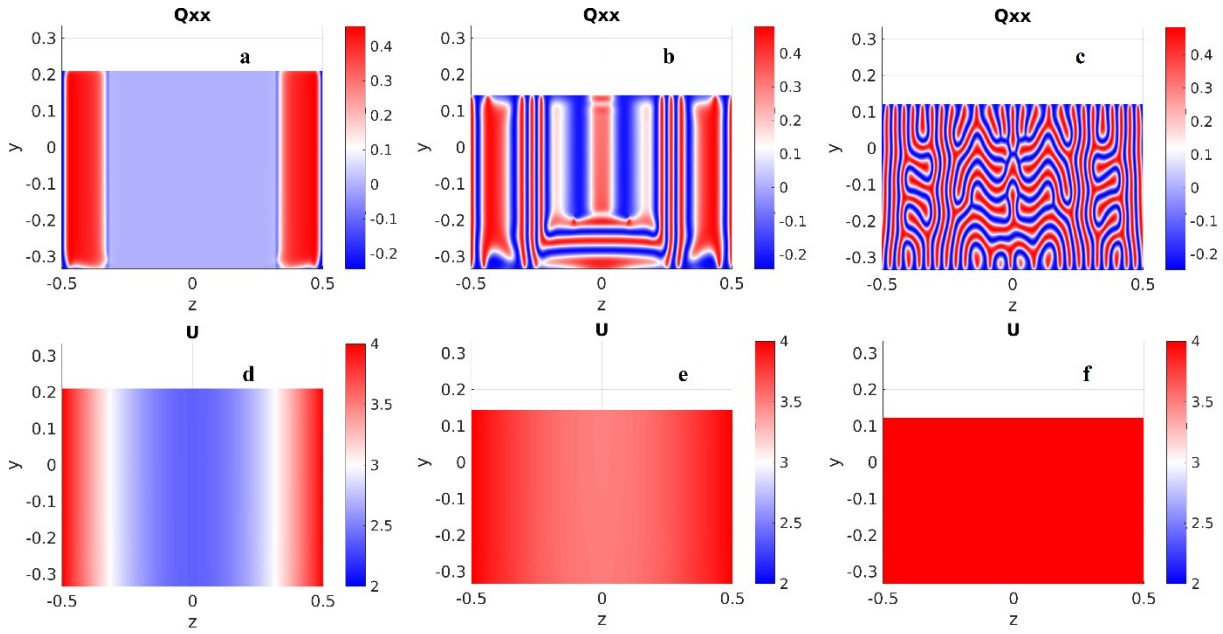

Figure S5. Q_{xx} surface plot in terms of the spatial coordinates *y*-*z* (a-c) for increasing times (t^* = 50, 200, 5000) and the nematic potential *U* (d-e) for the same times for $\Pi = 1\text{x}10^{-3}$, showing a homogeneous helical axis forming from the edge toward the central region of the cross section.

Next we focus on the cellular patterns obtained in the central region of the film when water removal rates are slow ($\Pi<\Pi^*$) . These cellular patterns correspond to distorted 2D blue phases and are common in the absence of 1D directed self-assembly [7]. Figure S6 shows and amplification of the polygonal structure obtained for the mono-domain/cellular mode ($\Pi<\Pi^*$) in terms of Q_{xx} (left) and S (right) where it is observed the latter vanishes at the vertices. The hexagonal cellular patterns is clear in the S-plot , which also shows a few penta-hepta defects [7] due to its random origin. The central region of each hexagon is characterized by the presence of non-singular core λ^{2+} disclination and by singular τ^- defects at the N vertices. The total topological defect charge C inside each cell follows Zimmer's rule [7]: $C = (N-2)/2$, which for N=6, yield C=2.

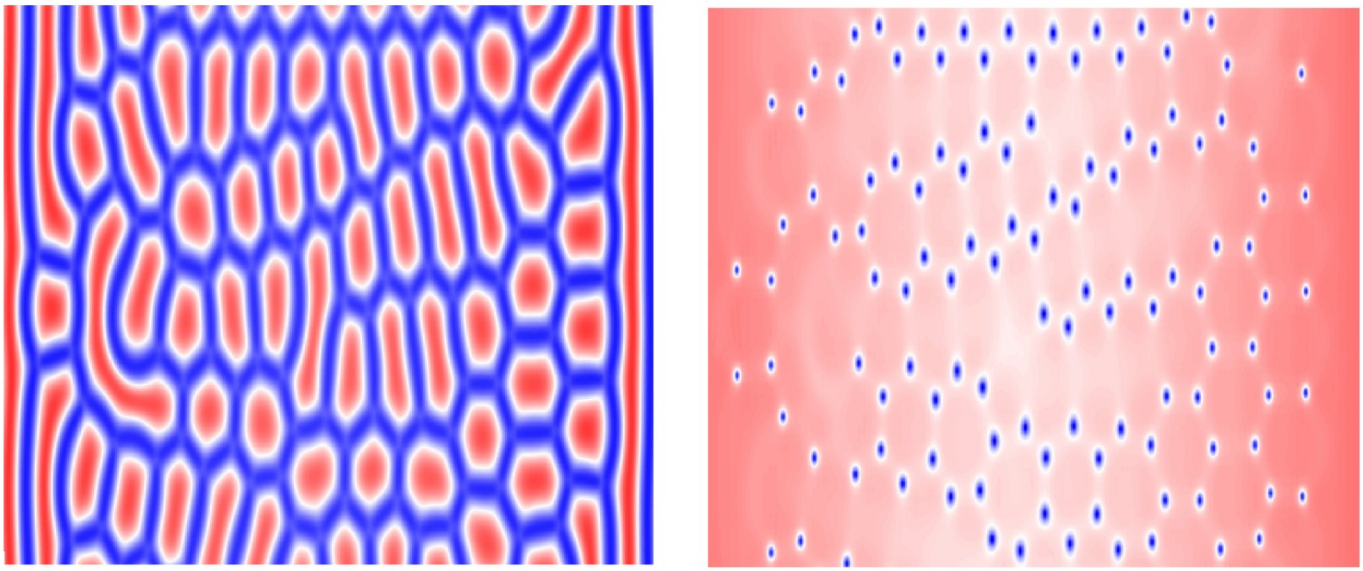

Figure S6. Amplification of the cellular region at the central region of the film for $\Pi = 10^{-5}$, in the monodomain-cellular mode.

Next we focus on the relation of the mass flux vector under synchrony (mondomain mode) and under slow water removal rate(monodomain-cellular mode). Figures S7 and S8 present the flux vector components J_y and J_z for $\Pi = 10^{-4}$ and 10^{-5} respectively for increasing times. The former shows the homogeneity in the mass flux vector components for all times of the simulations and the latter shows homogeneity for early times but inhomogeneity for later time. The non-negligible mass flux J_y in the vertical direction is an indication of the loss of stability of the planar 1D phase ordering front triggered by slow water removal rate.

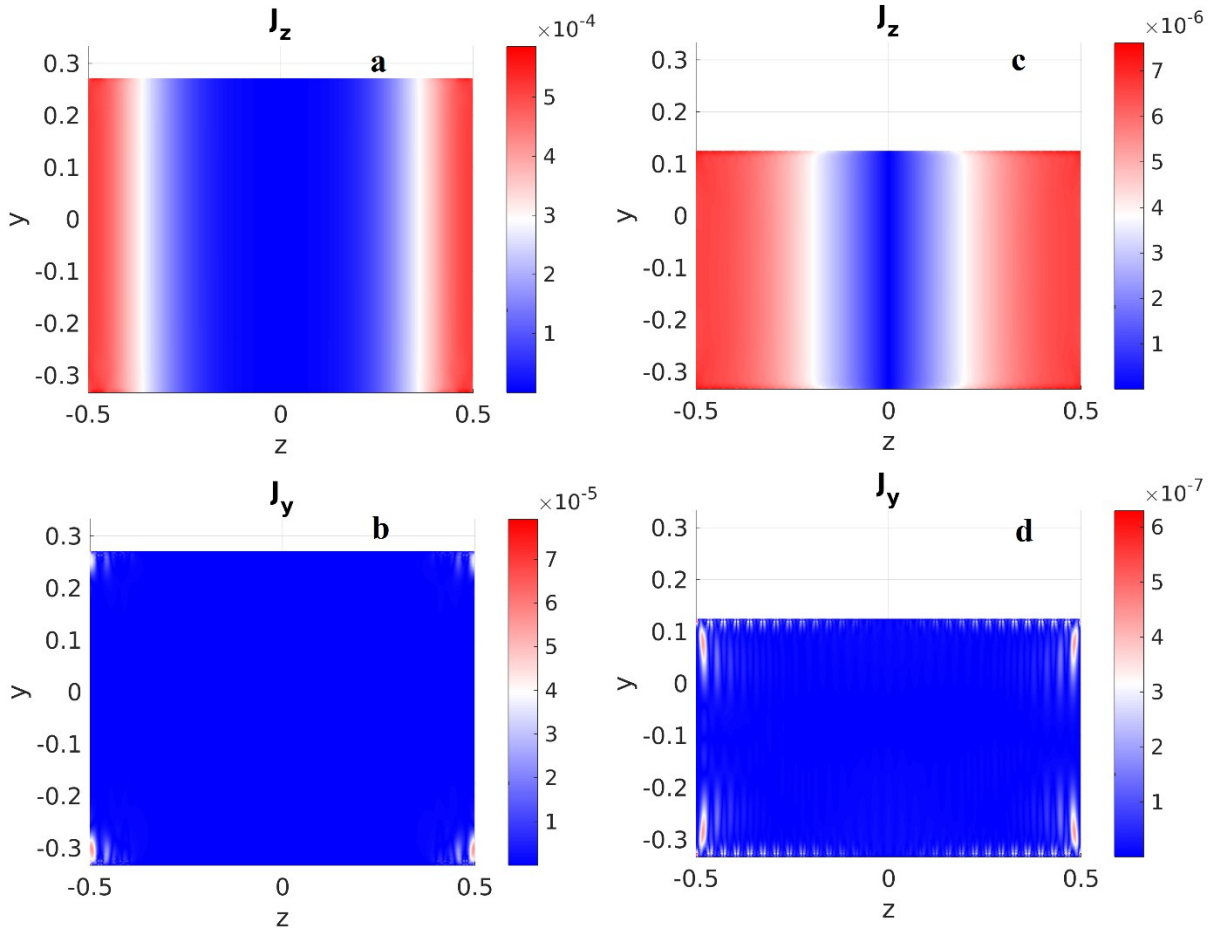

Figure S7. J_y and J_z components of the flux for $\Pi = \Pi^* = 10^{-4}$ (monodomain transition mode; perfectly synchronized water rate removal) at t = 100 (a-b) and t = 5000 (c-d) showing the homogeneity in the "z" component at all times and very weak contributions arising from the microstructure in the "y" component for late times.

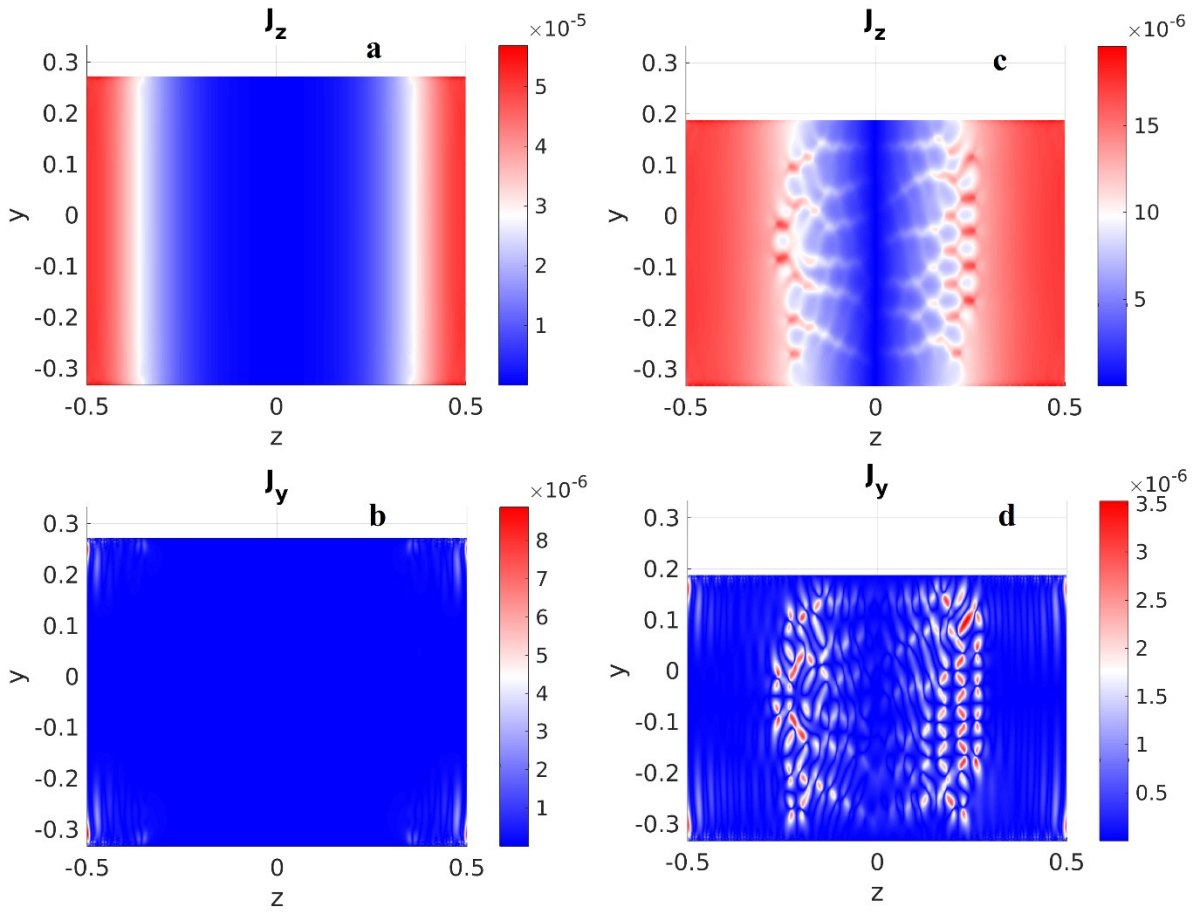

Figure S8. J_y and J_z components of the flux for $\Pi = 10^{-5} < \Pi^*$ (monodomain-cellular mode; slow water rate removal) , at t = 1000 (a-b) and t = 8000 (c-d) showing the homogeneity in the "z" component at early times and contributions arising from the microstructure in the "y" component at later times.